Coupling of rigorous multiphase flash with advanced linearization schemes for accurate compositional simulation

Abd, Abdul Salam; Abushaikha, Ahmad; Voskov, Denis

DOI
10.2118/203956-MS

Publication date
2021

Document Version
Final published version

Published in
Society of Petroleum Engineers - SPE Reservoir Simulation Conference 2021, RSC 2021

SPE-203956-MS

Coupling of Rigorous Multiphase Flash with Advanced Linearization Schemes for Accurate Compositional Simulation

Abdul Salam Abd and Ahmad Abushaikha, Division of Sustainable Development | College of Science and Engineering | Hamad Bin Khalifa University HBKU; Denis Voskov, Faculty of Civil Engineering and Geosciences, Delft University

This paper was prepared for presentation at the SPE Reservoir Simulation Conference, available on-demand, 26 October 2021 – 25 January 2022. The official proceedings were published online 19 October 2021.

Abstract

The properties of fluids flowing in a petroleum reservoir are quantified by understanding the thermodynamic behavior of each flowing phase in the system. This work describes proper techniques to formulate and execute a thermodynamic model for accurately predicting the equilibrium behavior of oil-gas-brine systems within the practical range of pressure and temperature. The three-phase flash algorithm is validated against published data from the available literature. The multiphase flash procedure is implemented to generate linearized physical properties by using an Operator Based Linearization (OBL) modelling technique allowing for a combination of multiple complex physics in the nonlinear solution of governing equations. This is the first implementation of three-phase flash calculations for hydrocarbons and brines based on fugacity-activity models coupled with an advanced highly efficient linearization scheme. Our approach increases the efficiency and flexibility of the modelling process of physical phenomena such as fluid flow in porous subsurface reservoirs.

Introduction

The costs of enhanced oil recovery (EOR) processes from hydrocarbon reservoirs have come down since 2014, and it accounts for 2% of global oil production (IEA, 2020). This share is increasing with the accessibility to new technology that helps engineers tap more of the available subsurface resources and the fact that many fields have become mature production provinces. However, implementing EOR comes with challenges on many fronts, such as the interactions between carbon dioxide and hydrocarbons that highlight the importance of multiphase equilibria, as vapor-liquid-liquid equilibrium is observed. This challenge is exacerbated by the fact that almost all reservoirs would have water content either from direct injection during secondary flooding or the presence of an aquifer in the formation. The presence of water causes an aqueous phase to form, and hence modelling multiphase equilibrium becomes more challenging yet essential in understanding the fluid flow of different phases in the subsurface reservoir.

In recent years, several methods have been proposed to achieve accurate phase-state identification of multi-component systems at a given temperature, pressure, and composition (Nasrifar & Moshfeghian,

2002; Reshadi et al., 2011). These phase behavior prediction techniques form an integral part in the development of compositional reservoir simulations, and thus as chemical equilibrium is accurately predicted, the fluid flow obtained from reservoir simulations is more reliable. Typically, the presence of water in hydrocarbons systems poses difficulties for multiphase equilibrium calculations at the level of stability tests and flash calculations convergence (Heidemann, 1974; Mokhatab, 2003; Neoschil & Chambrette, 1978; Peng & Robinson, 1980). Many researchers tend to thus neglect the presence of the aqueous phase in the compositional simulation and reduce the problem to two-phase flash only. Such an approach causes inconsistencies at the physical level, which may cause a serious error in simulation results, like CO_2 sequestration in the depleted gas or oil fields where the amount of CO_2 dissolved in the reservoir should be predicted by a full three-phase flash calculation.

The phase partitioning of hydrocarbon-brine systems is usually modelled by either using an equation of state (EOS) (Redlich & Kwong, 1949; Soave, 1972; Peng & Robinson, 1976) or an activity-based model that utilizes Henry's law (Li & Nghiem, 1986; Luks, Fitzgibbon & Banchero, 1976; Mehra, Heidemann & Aziz, 1982; Nghiem & Heidemann, 1982). In the former, the fugacity of each phase is typically calculated using a standard EOS such as modified Peng-Robinson (PR), Redlich-Kwong (RK), or Soave-Redlich-Kwong (SRK) that does not represent the presence of water in the system accurately. However, the second approach relies on an EOS to calculate the fugacities of the non-aqueous phase (liquid hydrocarbon and vapor gas), while an activity model is used to calculate the activity and Henry's coefficient of the aqueous phase (water). Both approaches are referred to as φ-φ (fugacity-fugacity) model and φ-γ (fugacity-activity) model respectively, where φ refers to the fugacity of the phase evaluated through and EOS while γ is the activity coefficient calculated through gas solubility modeling techniques.

The partitioning of the components in each phase is calculated using Rachdrod-Rice equations. These equations are solved to determine the phase composition and mole fractions for a given set of overall mole fraction and K values. (Li and Nghiem, 1982) argued that molar phase fractions could be allowed to go to negative values for two-phase mixtures in what they called the negative flash approach. This approach was extended by (Whitson and Michelsen, 1989) to show that the results of a two-phase negative flash can reliably substitute conventional phase stability testing. Extending the RR equations for multiphase equilibrium calculations, (Michelsen,1994) proposed a positive flash approach to solving the RR function where the molar phase fractions are kept within the physical boundaries ([0,1]). Later, (Leibovici and Nichita, 2008) developed the first multiphase negative flash approach with robust continuously differentiable functions when the physical phase boundaries are crossed. This approach was then followed by (Iranshahr et al., 2010a) work, where he suggested a generalized RR problem for an arbitrary number of phases with a robust nested bisection solution procedure. Although (Whitson and Michelsen, 1989) have shown the ability to detect phase instability using two-phase negative flash, performing a three-phase negative-flash is not enough to confirm the phase-state of single-or two-phase mixtures. Thus, (Iranshahr et al., 2010a) suggested using a multistage negative-flash approach to identify the phase-state of such compositions.

Thermodynamic equilibrium computations for phase split equilibrium have always been computationally demanding and impose many numerical complexities. Motivated to simplify these computations, a tie-simplex based parameterization method has been developed, which treats the thermodynamic problem using an extension of tie-simplices defined by equilibrium compositions. The work of (Voskov and Tchelepi, 2009) proposed parametrization of the compositional space based on tie-simplices and assembling them into a table to be later interpolated as a function of pressure. This approach is called isothermal Compositional Space Adaptive Tabulation (CSAT) methodology and is valid for an arbitrary number of phases. The CSAT was then generalized for thermal applications by (Iranshar et al.,2010b), where linear interpolation to obtain a tie-line for a composition with the specified pressure and temperature values and extended to realistic multiphase systems in (Iranshahr et al. 2012). The previous work formed the basis for Zaydullin

et al, (2012, 2016) to develop an adaptive compositional space-parameterization approach to represent governing differential equations in tie-simplex space, thus allowing for continuous representation of the phase envelope as a function of composition and pressure. Following these ideas, Voskov (2017) introduced an Operator-Based Linearization (OBL) technique to parameterize nonlinear terms (operators) in the governing equations using uniform mesh in the space of nonlinear unknowns. The developed operators are linearly interpolated during the course of the simulation on a mesh with predefined accuracy to speed up property calculations (including phase behavior evaluation) for multiple industrial applications (Khait and Voskov, 2018a,b; Kala and Voskov, 2020; Lyu et al. 2021). Moreover, the full details of implementing the OBL technique in an advanced parallel framework for reservoir simulation with high order discretization schemes such as Mixed Hybrid Finite Element method (MHFEM) and Mimetic Finite Difference (MFD) is discussed in details in our the work of (Abd and Abushaika, 2021; Abd et al., 2021; Nardean et al., 2020; Li et al., 2020; Abushaikha and Terekhov, 2020; Zhang and Abushaikha, 2019a,b; Hjieij and Abushaika, 2019a,b; Abushaikha et al., 2017) that we refer the reader to.

In general, the properties of fluids flowing in a petroleum reservoir are quantified by understanding the thermodynamic behavior of each flowing phase in the system. This necessitates that the composition of each phase should be known under the closing assumptions. This work describes new proper techniques to formulate and execute a thermodynamic model for accurately predicting the equilibrium behavior of oil-gas-brine systems within the practical range of pressure and temperature. This comprehensive thermodynamic model combines the φ-φ (fugacity-fugacity) and φ-γ (fugacity-activity) approaches to accurately perform three-phase flash calculations in the presence of aqueous brine. The model is implemented in a fully functioning reservoir simulator and parameterized using the OBL approach to solve the governing equations. The performance of the proposed model is validated for 1-D and 2-D meshes with highly heterogenous properties and provides accurate results for phase identification during the course of the simulations.

Theoretical Basis

The implementation of a φ-γ EoS-based model provides a more accurate determination of the aqueous phase behavior. The main challenge in calculating the phase split is determining how many phases are present in the mixture at a specific temperature and pressure. Typically, an explicit analysis of Michelsen's stability test is used (Baker, Pierce & Luks, 1982; Michelsen, 1982), where stationary points are located. The solution at these points is used to determine the stability of the system, but it requires multiple initial estimates of the equilibrium ratio (K) to avoid missing any instability regions.

To achieve thermodynamic equilibrium, the fugacity of each component in each phase should be equal. A generic equation could represent a three-phase system at equilibrium by,

$$f_i^V = f_i^L = f_i^{Aq} \tag{1}$$

where f_i is the fugacity of the vapor (V), liquid (L), or aqueous (Aq) phase, and i is the index of the component. The equation indicates that when three phases are present, their respective composition will keep changing until thermodynamic equilibrium is achieved. The equilibrium state is identified by calculating the equilibrium ratio k which is obtained by solving a typical Rashford-Rice (RR) equation (Rachford & Rice, 1952) using nested bisection (Iranshahr et al., 2010a) or Newton's method (Michelsen, Mollerup & Breil, 2008) that allows for detailed analysis of the composition of each component in each phase: liquid (x_i), vapor (y_i) and water (w_i) phases,

$$k_{xy} = \frac{y_i}{x_i} \tag{2}$$

$$k_{wy} = \frac{y_i}{w_i} \tag{3}$$

Next, we discuss Henry's law and fugacity computations for different phases and the implementation of stability analysis and phase split calculations.

Henry's Law

Henry's constant is used to model the solubility of gases in the aqueous phase and was suggested in multiphase flash calculations by (Li & Nghiem, 1986) and later modified by (Harvery, 1996). The correlation of Henry's law constants used in this work is defined by (Akinfiev & Diamond, 2003) with respect to given pressure and temperature,

$$\ln H_i = (1-\eta) \ \ ln \ \ f^0_{H_2O} + \eta \ln\left(\frac{RT}{Mw_{H_2O}}\rho^0_{H_2O}\right) + 2 \ \ \rho^0_{H_2O} \Delta B \tag{4}$$

where η is a constant for each gas component dissolved in the aqueous phase, $\rho^o_{H_2O}$ is the density of water and ΔB is the difference in the interaction between dissimilar molecules and that of identical solvent molecules. This interaction parameter is calculated from fitting experimental data into the correlation below,

$$\Delta B = \tau + \beta\left(\frac{10^3}{T}\right)^{0.5} \tag{5}$$

where τ and β are empirical constants calibrated experimentally for different components tabulated in Table 1 The input parameters for Henry's constant

Table 1—The input parameters for Henry's constant

Component	η	τ	β
CO2	−0.114535	−5.279063	6.187967
H2S	0.77357854	0.27049433	0.27543436
N2	−0.008194	−5.17537	6.906469
C1	−0.092248	−5.779280	7.262730
C2	−0.6091	−16.8037	20.0628
C3	−1.1471	−25.3879	28.2616
C4	−1.6849	−33.8492	36.1457

Calculation of molar volume of water. The molar volume of water V_{mH_2O} is estimated by the correlation of (Fine & Millero, 1973),

$$V_{mH_2O} = V^0 - \frac{V^0_{mH_2O} P}{B + A_1 P + A_2 P} \tag{6}$$

where the constant parameters $V^0_{mH_2O}$, A_1, A_2 and B are defined as,

$$V^0 = \frac{1 + 18.159725\times10^{-3}T}{(0.9998396 + 18.224944\times10^{-3}T - 7.922210\times10^{-6}T^2 - 55.44846\times10^{-9}T^3 + 149.7562\times10^{-12}T^4 - 393.2952\times10^{-15}T^5)} \tag{7}$$

$$A_1 = 3.2891 - 2.3910\times10^{-3}T + 2.8446\times10^{-4}T^2 - 2.8200\times10^{-6}T^3 + 8.477\times10^{-9}T^4 \tag{8}$$

$$A_2 = 6.245\times10^{-5} - 3.913\times10^{-6}T - 3.499\times10^{-8}T^2 + 7.942\times10^{-10}T^3 - 3.299\times10^{-12}T^4 \tag{9}$$

$$B = 1.9654.320 + 147.037T - 2.21554T + 1.0478\times10^{-2}T^3 - 2.2789\times10^{-5}T^4 \tag{10}$$

and the temperature, T is in degrees Celsius.

The density can be easily defined then as,

$$\rho_{H_2O} = \frac{1}{V_{mH_2O}} \tag{11}$$

Calculation of water saturation pressure. Water saturation pressure is obtained using a correlation of (Saul & Wagner, 1987) as reported by (Shibue, 2003),

$$ln\ \ P_s = \frac{T_c \ln P_c}{T}\ \left[a_1\tau + a_2\tau^{1.5} + a_3\tau^3 + a_4\tau T_c^{3.5} + a_5\tau^4 + a_6\tau^{7.5}\right] \tag{12}$$

where T_c and P_c are the critical pressure and temperature of the water component, while $\tau = 1 - \frac{T}{T_C}$. The empirical constants are reported in **Table 2** The input parameters for the molar volume correlation.

Table 2—The input parameters for the molar volume correlation

Component	a_1	a_2	a_3	a_4	a_5	a_6
H2O	−7.85951783	1.84408259	−11.7866497	22.6807411	−15.9618719	1.80122502

The saturation pressure can also be calculated by the semi-empirical equation of (Frost & Kalkwarf, 1953), which requires more parameters but gives fairly similar results to (Saul & Wagner, 1987).

Calculation of water component fugacity in the aqueous phase. The equation of (Kinget al., 1992) is applied to obtain saturated reference water fugacity,

$$f^0_{H_2O} = P_s e^{\frac{V_{mH_2O}(P-P_s)}{\rho_{H_2O}RT}} \tag{13}$$

Fugacity Computation

Liquid and vapor phases. The fugacity of the liquid and the vapor phase is calculated using the Peng-Robinson (PR) EOS defined as:

$$P = \frac{RT}{V_m - b} - \frac{a\alpha}{V_m^2 + 2bV_m - b^2} \tag{14}$$

where,

$$a = 0.45724\frac{R^2T_c^2}{P_C}$$

$$b = 0.07780\frac{RT_c}{P_c}$$

$$\alpha = \left(1 + \kappa\left(1 - \sqrt{T_r}\right)\right)^2$$

$$\kappa = 0.37464 + 1.54226\omega - 0.26992\omega^2, \quad \omega < 0.5$$

$$\kappa = 0.3796 + 1.485\omega - 0.1644\omega^2 + 0.01667\omega^3 \ , \quad \omega \geq 0.5$$

The parameter ω represents the acentric factor of the species, while R is the gas constant. The critical temperature and pressure are denoted by T_C and P_C respectively. The cubic equation is solved by writing it in an expanded form to represent the compressibility factor, Z as follows:

$$Z^3 - (1 - B)Z^2 + (A - 2B - 3B^2)Z + (AB - B^2 - B^3) = 0 \tag{15}$$

where,

$$A = a\alpha\frac{P}{R^2T^2}$$

$$B = b\frac{P}{RT}$$

The following composition-dependent mixing rule is applied to calculate a and b,

$$a = \sum x_i a_{ij} \tag{16}$$

$$a_{ij} = \sqrt{a_i a_j} \sum x_j \left(1 - k_{ij}\right) \tag{17}$$

$$b = \sum x_i b_{ij} \tag{18}$$

where k_{ij} is the binary interaction coefficients determined from experimental values of mixtures.

The fugacity coefficient of each component can be hence calculated using the equation:

$$\ln\phi_i = \frac{b_i}{b}(Z-1) - \ln(Z-B) - \frac{1}{\delta_2 - \delta_1}\frac{A}{B}\left(\frac{2a_{ij}}{a} - \frac{b_i}{b}\right)\ln\left(\frac{Z+\delta_2 B}{Z+\delta_1 B}\right) \tag{19}$$

where δ_1 and δ_2 are empirical constant for PR-EOS defined as $1-\sqrt{2}$ and $1+\sqrt{2}$ respectively.

The result of the fugacity calculation is used to obtain a new equilibrium ratio k_i that is updated at each iteration level using the following relation:

$$k_i^{n+1} = K_i^n \frac{f_{Li}^n}{f_{Vi}^n} \tag{20}$$

Aqueous phase. The water-rich phase is modelled using an activity model that is based on Henry's law constants. The fugacity of the aqueous phase is reported in (Spycher & Pruess, 2005) as,

$$f_i^{aq} = w_i H_i \gamma_i \tag{21}$$

where H_i is henry's constant γ_i is the activity coefficients and w_i is the molar fraction of each component in the aqueous phase.

We note that the fugacity coefficient of the components in the aqueous does not depend on the molar composition,

$$\phi_i = \frac{H_i}{P} \quad i \neq w \tag{22}$$

Combining the fugacity expression for fugacities in the vapor and water-rich phase yield a thermodynamic equilibrium relationship expressed as follows,

$$w_i H_i \gamma_i = P \phi_i y_i \tag{23}$$

Activity Coefficient

The activity coefficient is calculated using a correlation by (Rogers & Pitzer, 1982) to account for the deviation of a certain mixture from ideality. Pitzer's relation is reliable for high salt content solutions, and this is important since the activity coefficients are highly influenced by the anions, cations, and interactions between particle pairs. The model is represented by,

$$\ln\gamma_i = \sum_c 2m_c\lambda_{i-Na} + \sum_c 2m_a\lambda_{i-Cl} + \sum_c\sum_a 2m_a m_c \xi_{i-Na-Cl} \tag{24}$$

where m_c is the cation molality, m_a is the anion molality, $\lambda_{i\text{-}Na}$ and $\lambda_{i\text{-}Cl}$ are the second-order parameters representing cations and anions, and $\xi_{i\text{-}Na\text{-}Cl}$ is a third order parameter dependent on pressure and temperature. The parameters $\lambda_{i\text{-}Cl}$is assumed to be zero for NaCl dissolved in solutions. The parameters $\lambda_{i\text{-}Na}$ and $\xi_{i\text{-}Na\text{-}Cl}$ are estimated using the following correlation with the relevant constants tabulated in **Table A-1** Pitzer parameters for the second-order parameter $\lambda_{i\text{-}Na}$ of the activity coefficients and **Table A-2** Pitzer parameters for the third-order parameter $\xi_{i\text{-}Na\text{-}Cl}$ of the activity coefficients of Appendix A respectively.

$$X(T,P) = c_1 + c_2 T + \frac{c_3}{T} + c_4 P + \frac{c_5}{P} + c_6\frac{P}{T} + c_7\frac{T}{P^2} + c_8\frac{P}{630-T} + c_9 T\ln P + C_{10}\frac{P}{T^2} + c_{11}P^2 T + c_{12}PT \tag{25}$$

Phase Split Calculations

The flash procedure is used to determine the composition of each phase in a certain system. Typically, the computations are carried out at constant pressure and temperature to determine the unknown variables F_j and x_{ij} representing the molar ratio of each phase in the system and the mole fraction of a component i is phase j respectively. If N_p is the total number of phases and N_c is the number of components, then the total number of unknows is represented by $N_P + N_P N_c$.

The phase composition and the phase distributed should both add to unity, and the overall composition can be written as,

$$z_i = \sum_{j=1}^{N_p} x_{ij} F_j \tag{26}$$

The equilibrium ratio, K, is generally defined to reference phase 1 as,

$$K_{j1} = \frac{x_{ij}}{x_{i1}} \tag{27}$$

The K values are updated using a successive substitution scheme to minimize the Gibbs energy of the system by utilizing the fugacity coefficients of the three phases.

Stability Analysis

The successive substitution method (SSI) is used to update and solve both the stability and flash calculations in our suggested scheme. The RR equations are handled though a generalized negative flash strategy developed by (Iranshar et al., 2010a). This method can be labelled as mathematically abstract as it allows for phase fraction to be negative

In stability analysis, the initial guess of the equilibrium ratios greatly affects the number of minimum points in the TPD function or in other words its local minimization process. This means that instability might go undetected if the system is not initialized properly. In some cases, improper initialization might lead to convergence problems in the phase split calculations as well. Based on the work (Michelsen, 1952; Baez et al., 2007; Li and Firoozabadi, 2012), Nc+4 sets on initial K guesses is suggested. If we have a two-phase system of vapor and hydrocarbon liquid, Wilson correlation and its inverse are applied as initial guesses for stability analysis like most commercial simulation software. The (Wilson, 1968) formula is written as,

$$K_i^{wilson} = \frac{P_{ci}}{P} \exp\left[5.371\left(1+\omega_i\right)\left(1-\frac{Tc_i}{T}\right)\right] \tag{28}$$

where T_{ci}, P_{ci} and ω_i are the critical temperature, critical pressure and acentric factor of component i.

However, when an aqueous phase is present in the system, Wilson's correlation becomes unreliable. The following set of K_i^{stab} values is suggested to increase the possibility of selecting appropriate initial K values,

$$K_i^{stab} = \left[\left\{K_i^{wilson}\right\}, \left\{\frac{1}{K_i^{wilson}}\right\}, \left\{\sqrt[3]{K_i^{wilson}}\right\}, \left\{\frac{1}{\sqrt[3]{K_i^{wilson}}}\right\}, \left\{K_i^{pure}\right\}\right] \tag{29}$$

where,

$$\begin{cases} K_i^{pure} = \frac{0.9}{z_i} \\ K_j^{pure} = \frac{0.1}{(N_c - 1) z_j} \quad (j \neq i) \end{cases}$$

In our system, and since an activity model is implemented, we obtain an initial estimate of the equilibrium constant between the vapor and aqueous phase from the work of (Ballard, 2002) and adopted by (Wapperom, 2019),

$$y_i P\phi_{iv} = w_i \gamma_{iw} p_i^{sat} \exp\left(\int_{p_i^{sat}}^{P} \frac{v}{RT} dP\right) \tag{30}$$

where w_i and y_i are the liquid and vapor mole fraction of component i respectively, ϕ_i is the fugacity coefficient, γ_i is the activity coefficient and p^{sat} is the saturation pressure. We assume that an infinite dilution activity coefficient is presentable of the component in the aqueous phase due to the high dilution. Furthermore, the Poynting factor (exponential term) and the vapor fugacity coefficient are assumed to be equal to unity for simplification, thus reducing the equation to,

$$K_{iw} = \frac{y_i}{w_i} = \frac{p_i^{sat}}{p} \gamma_{iw}^{\infty} \tag{31}$$

The saturation pressure is calculated according to the following correlation,

$$p_i^{sat} = P_{ci} exp\left[a_1 + \omega_i a_2\right] \tag{32}$$

The constants a_1 and a_2 are temperature dependent and are calculated using the parameters in **Table 3**,

$$a_1 = a_{11} + a_{12}\frac{T_{ci}}{T} + a_{13}\ln\frac{T}{T_{ci}} + a_{14}\frac{T^6}{T_{ci}^6} \tag{33}$$

$$a_2 = a_{21} + a_{22}\frac{T_{ci}}{T} + a_{23}\ln\frac{T}{T_{ci}} + a_{24}\frac{T^6}{T_{ci}^6} \tag{34}$$

Table 3—The input parameters used to calculate the saturation pressure for different components

a_{11}	a_{12}	a_{13}	a_{14}	a_{21}	a_{22}	a_{23}	a_{24}
5.927140	−6.096480	−1.288620	0.169347	15.25180	−15.68750	−13.47210	0.43577

The saturation pressure of water is calculated separately using Antoine equation with the empirical constants listed in **Table**.

$$p_i^{sat} = exp\left[a_1 + \frac{a_2}{T + a_3}\right] \tag{35}$$

Table 4—The input parameters used to calculate the saturation pressure for water

a_1	a_2	a_3
12.048399	4030.18245	−38.15

The activity coefficient at infinite dilution for water is equal o unity while the other computed are computed using,

$$\gamma_i^{\infty} = exp\left[a_1 + a_2 N_i + \frac{a_3}{N_i}\right] \tag{36}$$

The parameters N_i represents the number of carbon atoms in each component, and the constants to calculate infinite dilution activity coefficient are tabulated in **Table 5**.

Table 5—The input parameters used to calculate the infinite dilution activity coefficient

a_1	a_2	a_3
0.688	0.642	0

If a vapor-liquid (V-L) stability is carried out, $\{K_i^{wilson}\}$ and $\left\{\frac{1}{K_i^{wilson}}\right\}$ are sufficient as initial estimates. Other stability tests as vapor-water (V-W) and liquid-water (L-W) requires the full set of K_i^{stab} in addition to $K_i^{activity}$ to initialize the system properly.

Model Validation and Applied Reservoir Simulation Cases

In this section, we present a brief comparison of the performance of the implemented code for a three-phase system and compare the results with published models from the literature. We then test the proposed thermodynamic model for 1-D and 2-D reservoir simulation cases using the OBL scheme.

Ternary Diagram of a C_1- nC_{10} -H_2O mixture (3-phase system)

In the work of (Iranshar et al., 2010a), a full PR-EOS approach is used to establish and calculate the thermodynamic equilibrium between the vapor, liquid, and the aqueous phases. Initially, a three-phase negative-flash is performed. If the composition is inside the tie triangle(three-phase), its state is confirmed. Otherwise, based on the results of the three-phase negative-flash, additional two-phase negative-flash computations are necessary. This approach does not determine with confidence the number of phases in each region as stability testing is not performed. Opposed to our suggested approach, the (Iranshar et al., 2010a) approach would not be able to appropriately characterize the dissolution of gasses into the aqueous phase as only EoS models are used. The full PR-EOS approach shows the tie-triangle eventually degenerates into a line at a pressure of 170.53 bar, while the activity approach shows that the three-phase region is maintained at that pressure and only degenerates at around a pressure of 192 bar, see **Fig. 1**. The prediction of the aqueous phase using an EoS model is challenging and does not provide accurate representation of the system's thermodynamic state as certain conditions. Thus, the degeneration of the tie triangle is noticed at a higher pressure when compared to (Iranshar et al., 2010a) approach.

Analysis of 1-D and 2-D Reservoir Simulations

The objective of this analysis is to couple the three-phase activity-based flash model with the transport equations in a reservoir using an advanced highly efficient linearization scheme named Operator Based Linearization (OBL) (Voskov, 2017). The governing equations for the multiphase flow of a fluid in a porous medium are given by the conservation of mass, Darcy's law, and an equation of state. It is assumed that the diffusion and dispersion forces are very small so they can be neglected. The continuity equation is as follows,

$$F_i = \frac{\partial N_i}{\partial t} + L_i = 0 \tag{37}$$

where F_i is the residual function that should amount to zero after the system to converges to an acceptable solution, $\frac{\partial N_i}{\partial t}$ is the accumulation term and L_i is the flux term.

The term N_i refers to the total molar mass of fluid species i, and is defined as:

$$N_i = \sum_{j=1}^{n_p} (\rho_j \phi S_j X_{ij}) \tag{38}$$

where n_p is the number of fluid phases, ρ_j is the density of phase j that depends on pressure, temperature, and molar fraction, ϕ is the porosity and X_{ij} is the mole fraction fluid species i in the fluid phase j.

Also, the flux term L_i incorporates the effects of different transport phenomena, including advective, diffusive and dispersive processes as well as the well source term:

$$L_i = \nabla \cdot \sum_{j=1}^{np} (\rho_j X_{ij} \mathbf{u_j} - \rho_j \phi S_j \mathbf{D_{ij}} \nabla X_{ij}) + q_i^W \tag{39}$$

where $\mathbf{u_j}$ is the velocity for phase j, D_{ij} is the dispersivity tensor for fluid species i in phase j, q_i^W is the well rate of species i

The velocity $\mathbf{u_j}$ is given by Darcy's law:

$$\mathbf{u_j} = -\mathbf{K}\frac{k_{rj}}{\mu_j}\left(\nabla p_j + \rho_j g\right) \tag{40}$$

Where K is the rock permeability, k_{rj} is the relative permeability of phase j, p_j is the pressure of phase j, and g is the acceleration of gravity.

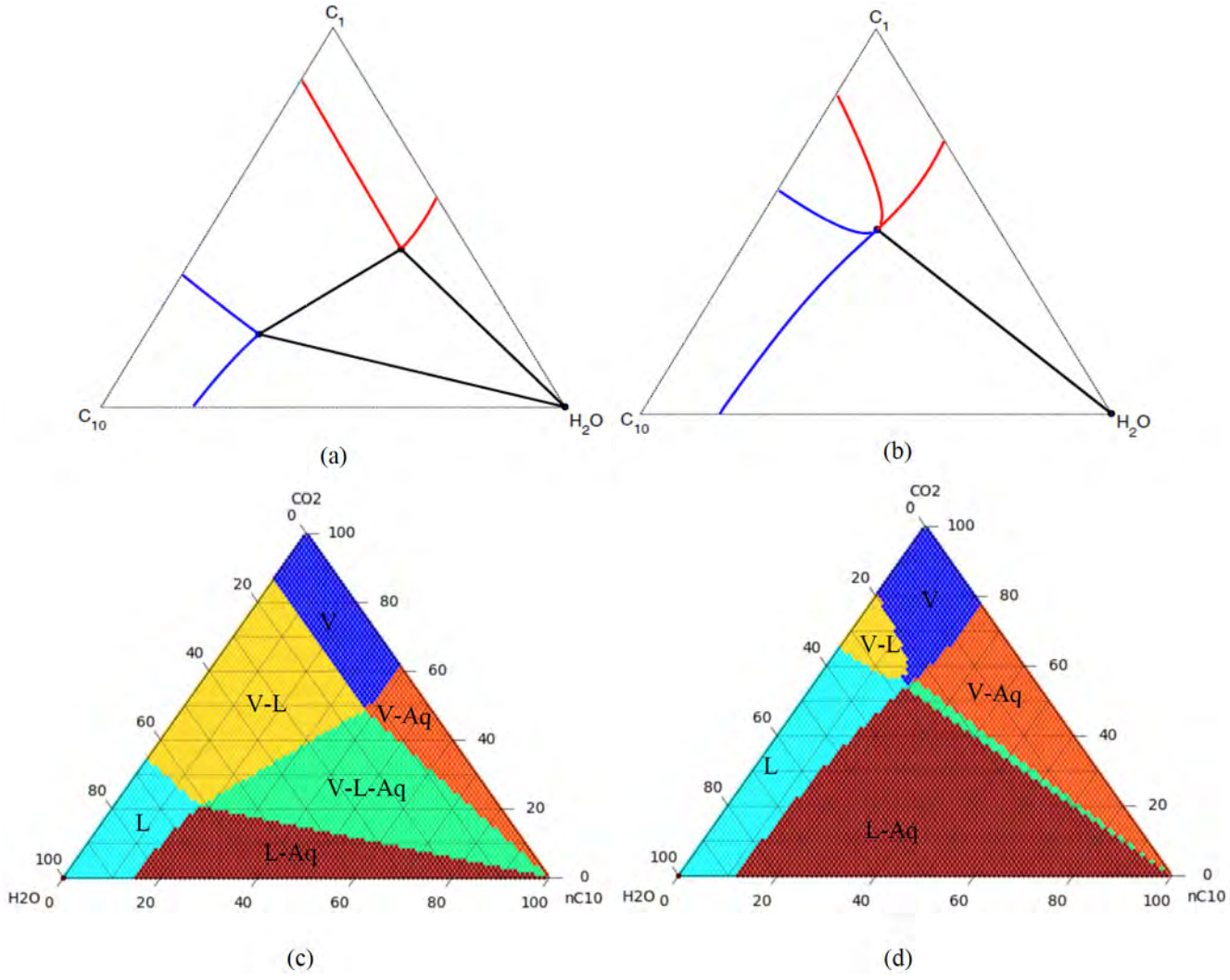

Figure 1—Complete parameterization of {H2O, C1, C10} at T = 520 K, (a) and (c) p = 100 bar and (b) and (d) tie-triangle degeneration at p = 170.53 bar and p=192 respectively. The diagrams in (a) and (b) are adapted from (Iranshar et al., 2010a) while (c) and (d) are generated using the package described in this paper

These equations are general in their applicability, where each component may exist in any or all of the three-phase equations. The governing equation is discretized and re-written in term of state-based (physical properties of fluid and rock) and space-based (properties transformed in space) operators following the OBL approach:

$$V\phi_0\left[\alpha_i(\omega)-\alpha_{ci}(\omega_n)\right]-\Delta t\sum_{l\in L(i)}\sum_{j=1}^{np}\left(\Gamma^l\beta_{ij}^l(\omega)\Delta\Phi_j^l+\Gamma_d^l\gamma_{ij}^l(\omega)\Delta\varepsilon_{ij}\right)+\theta(\xi,\omega,u) \quad (41)$$

Where,

- ω is a state-dependent parameter
- ξ is a space-dependent parameter
- $\alpha_c(\omega)=\left(1+c_r\left(p-p_{\text{ref}}\right)\right)\sum_{j=1}^{np}x_{ij}\rho_j s_j$
- $\beta_{ij}(\omega)=x_{ij}\,\rho_j k_{rj}/\mu_j$
- $\gamma_{ij}(\omega)=(1+c_r(p-p_{\text{ref}}))\rho_j s_j D_{ij}$
- $\varepsilon_{ij}(\omega)=x_{ij}$
- $\theta(\xi,\omega,u)=\Delta t\sum^{np}x_{ij}\rho_j q_j(\xi,\omega,u)$

The parameters ω and ω_n are nonlinear unknowns in the current and previous timestep, respectively; $\theta(\xi, \omega, u)$ is the source term; V, ϕ_0 and c_r are initial volume, porosity and rock compressibility, respectively; Φ_j^l is the phase pressure difference between neighbor cells; and Γ^l and Γ_d^l are the space-dependent part of convective and diffusive transmissibility, respectively.

For the subsequent tests, we simulate various injection scenarios in two different meshes (1-D and 2-D) and project the injection and production conditions on the ternary diagram of an nC_{10} - CO_2 - H_2O mixture. The first mesh is in 1-D and is composed of 1000 cells in the x-direction with an injector and a producer being placed at the far ends of the grid, see **Fig. 2**. The permeability is scalar at a value of 1000 md in the x and y directions and 10 md in the z-direction with a domain porosity of 0.3. On the other hand, the second mesh is taken as the seventh layer of the SPE-10 model, see **Fig. 3**, with four producers are around the corners while the injector is placed in the middle. The mesh is 60x220x1 with porosity and permeability being highly heterogenous, see **Fig 4**.

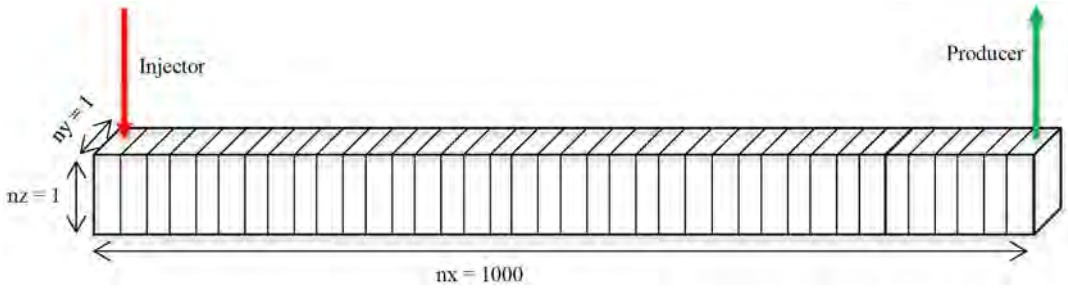

Figure 2—A simple 1-D mesh with a producer and an injector located at the far ends

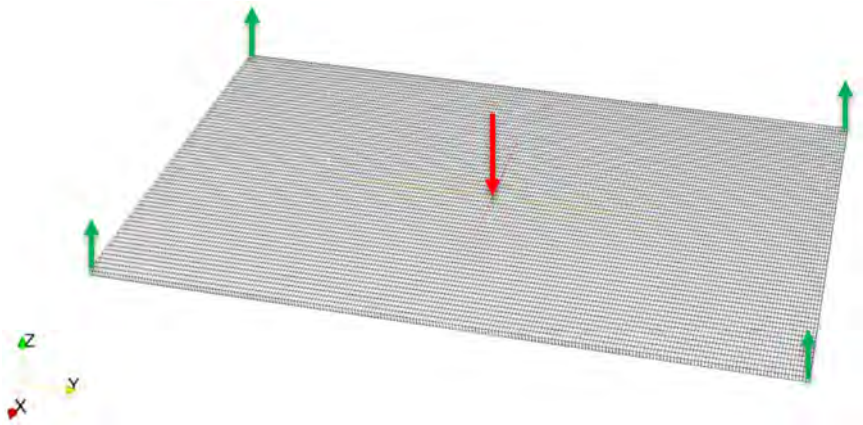

Figure 3—A 2-D mesh representation of the seventh layer of SPE-10 model. The injector is shown in red while the producers are shown in green.

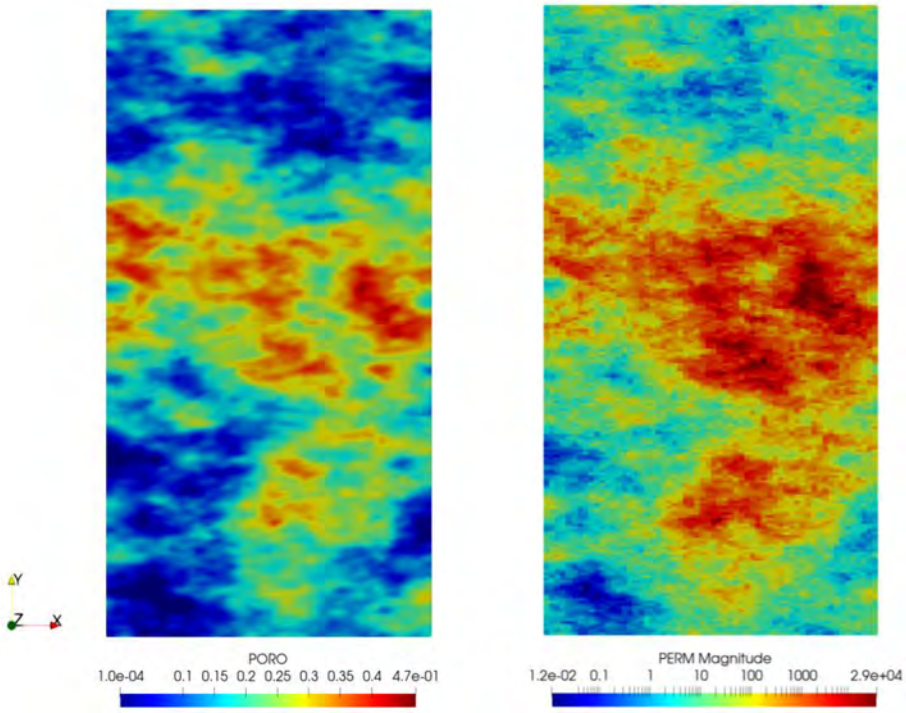

Figure 4—The porosity (left) and permeability (right) 2-D distribution maps for the seventh layer of SPE-10 model

Test I – Pure CO_2 Injection. We initialize the 1-D and 2-D models with a Decane-Carbon Dioxide-Water mixture at a pressure and temperature of 100 bar and 400 K respectively. The injector well is used to inject pure CO_2 at 120 bar while the producers are operating at an average pressure of 80 bar. The ternary diagram of the nC10- CO_2- H_2O mixture at the given condition is generated using the multiphase flash package, see **Fig 5**. The injection and production conditions are shown on the diagram as red and green points respectively. The maps in **Fig. 6** show the progression of the composition of each component in the reservoir as the simulation ceases, along with the final pressure distribution across the cells.

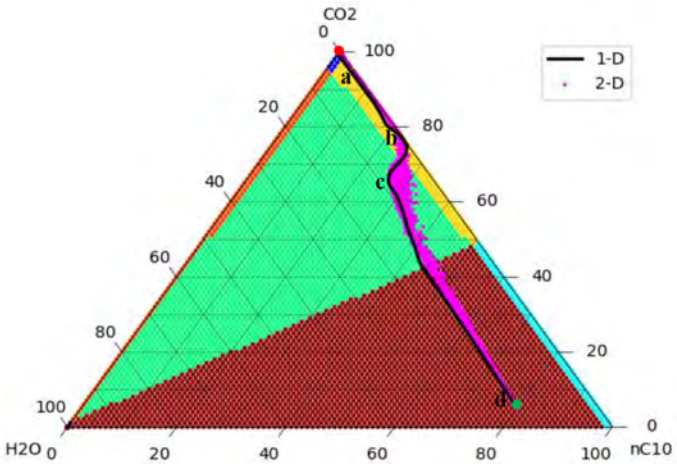

Figure 5—Ternary phase diagram for a nC10- CO2 – H2O system with constant Pressure and Temperature at 100 bar and 400 K respectively. The injection path is drawn between the injection condition (red point) and the initial reservoir condition (green

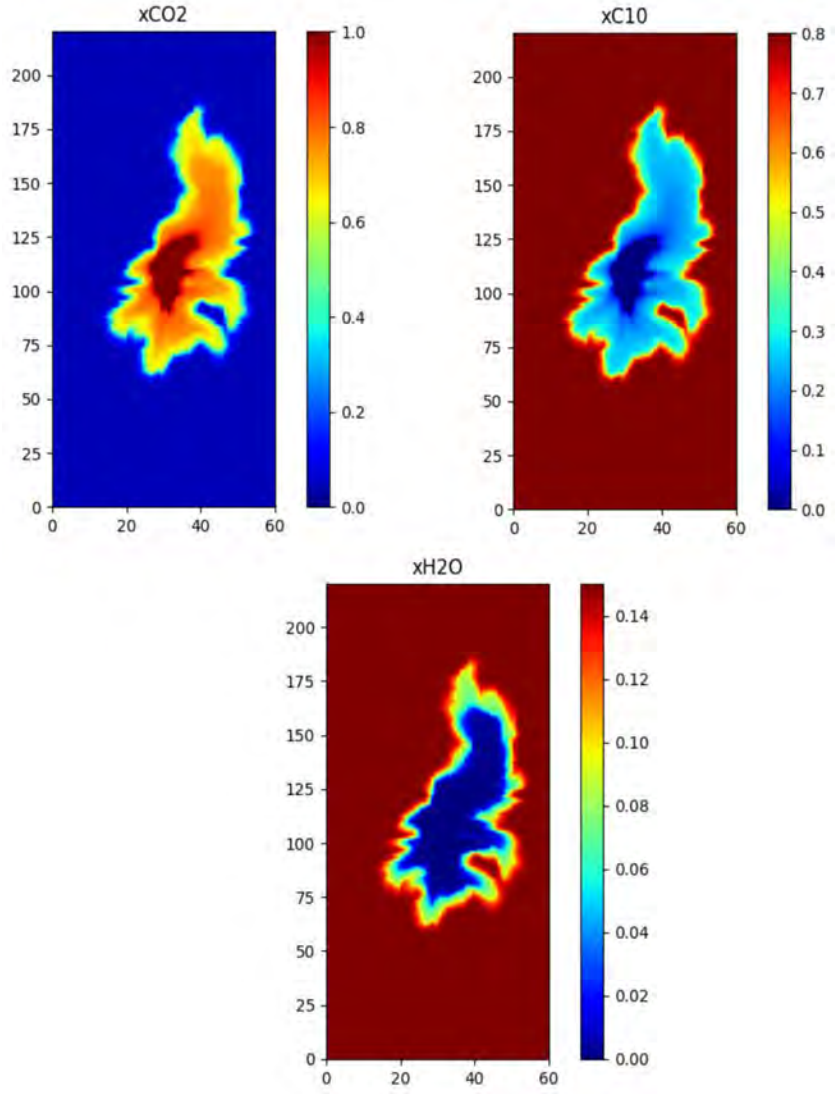

Figure 6—The saturation maps of the reservoir components at a simulation time of t=3500 days. The flow tends to move to the region of the highest permeability and towards the four producer wells.

The concentration distribution of each component is plotted against the distance traveled at the end of each simulation and is shown for both the 1-D and 2-D models in **Fig. 7-a** and **Fig. 7-b** respectively. The profiles are visualized in the x-direction for the 1-D, and against a horizontal line starting from the injector to the right side of the mesh in the 2-D case. We notice that composition profiles are almost similar for both models with the points **a, b, c**, and **d** on the ternary diagram featuring the main shocks. The solution route starts at pure CO_2 composition then enters the two-phase (V-L) region with a shock from the injection condition **a** across the curve to point **b**. As **Fig. 5** shows, point **b** lies on a tie line that extends through point **a**. At point **c**, the solution route switches to the non-tie-line path as it enters to the three-phase (V-L-Aq) region. After that, another shock is noticed as the path enters a two-phase (L-Aq) region and reaching to point **d** at the initial reservoir conditions.

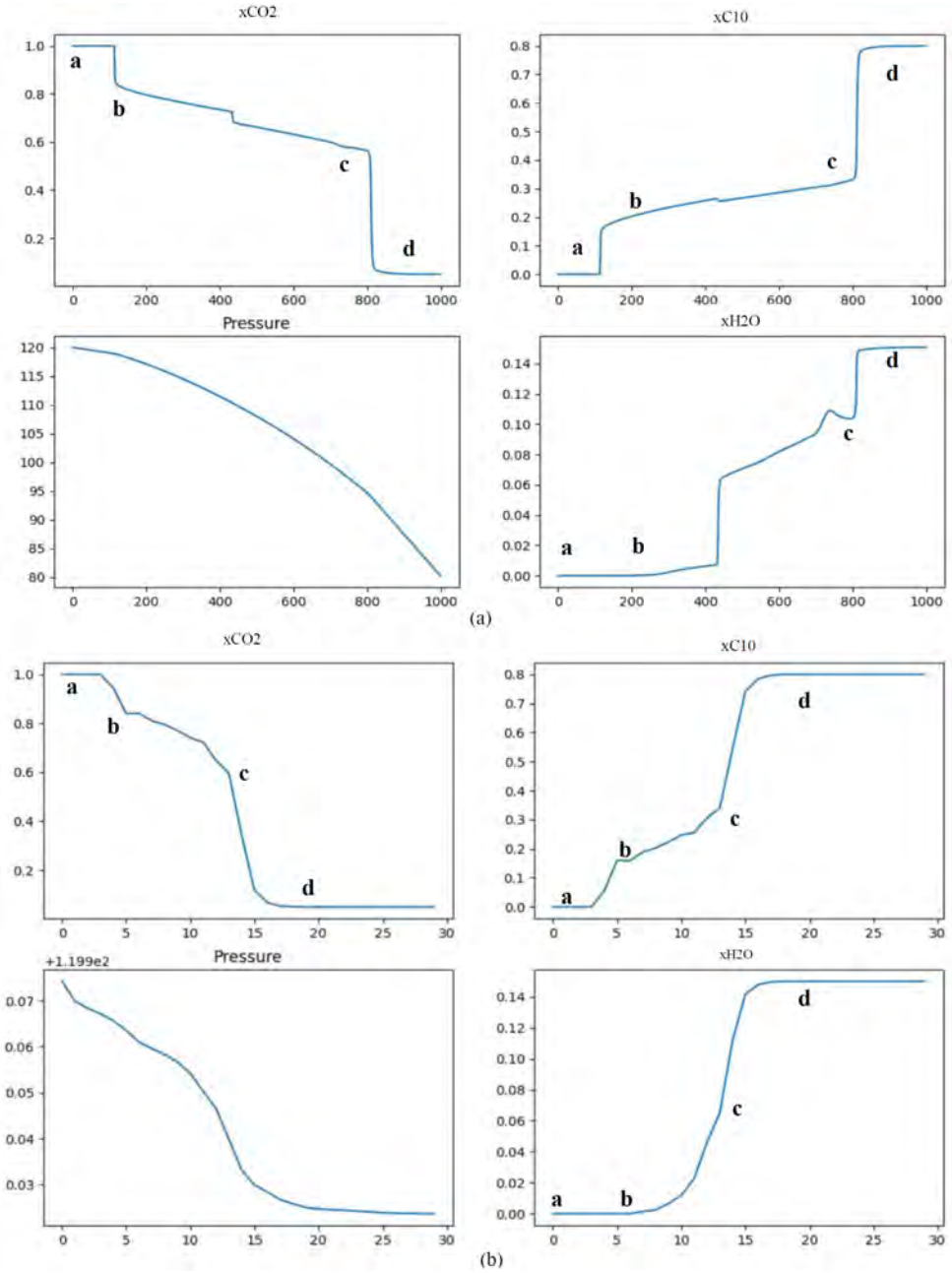

Figure 7—Test I solution profiles of composition and pressure with distance at the end simulation time for (a) 1-D model and (b) fixed trajectory in the 2D layer of SPE10 model

The concentration maps of **Fig. 7** show that the nC_{10} concentration increases steadily as the solution path is traced from the injection composition to the initial composition upstream where this profile mirrors that of the oil saturation in the reservoir. The profile pattern for CO_2 is similar to an inverted version of the profile for nC_{10} where the concentration declines monotonically as the solution path is traced, and the CO_2 concentration drops to zero behind the trailing shock (**c-d**).

Test II – Injection of 50:50 mixture of CO_2 and H_2O. In this test, we inject a mixture of CO_2 and H_2O into a reservoir with the same initial composition tested previously. The reservoir sits at 100 bar and 450 K for pressure and temperature respectively, and these conditions do not change between the 1-D and 2-D models. The ternary diagram at the provided conditions is visualized in **Fig. 8**. We notice that the pure CO_2 (blue), V-L (yellow), and V-Aq (orange) regions are significantly larger compared to the previous due to the increase in the temperature. The variations in the composition and the pressure at the final time are shown in **Fig. 9**.

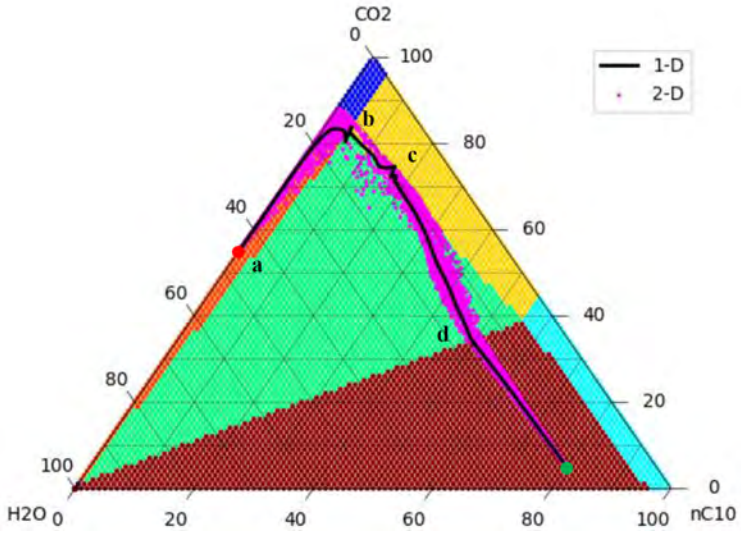

Figure 8—Ternary phase diagram for a nC10- CO2 – H2O system with constant Pressure and Temperature at 100 bar and 450 K respectively. The injection path is drawn between the injection condition (red point) and the initial reservoir condition (green)

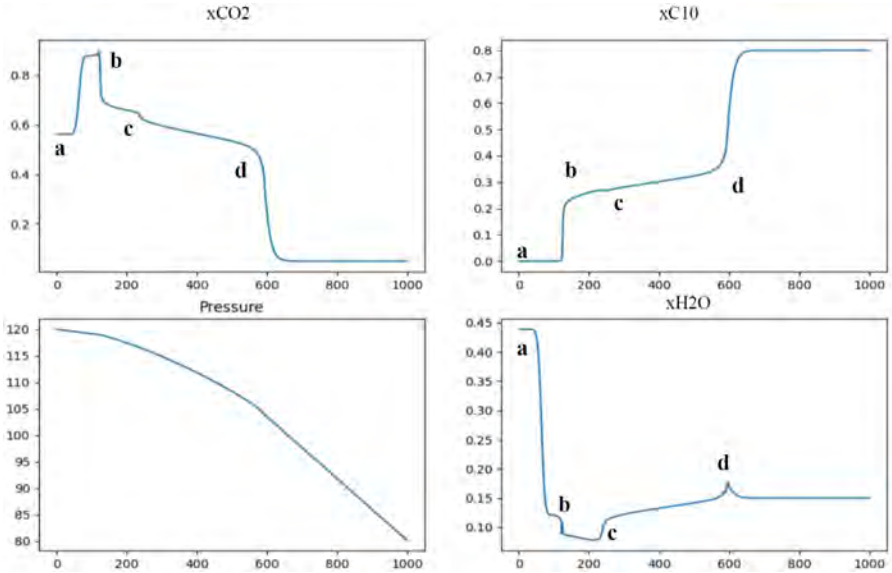

Figure 9—The saturation maps of the reservoir components at a simulation time of t=6500 days. The area around the injector is fully swept as shown by the residual nC10 map.

At the injection conditions, CO_2 and H_2O start accumulating with CO_2 mobilizing faster due to its lower density. It is noticed that the total injection path for both the 1-D and 2-D models are virtually similar. Initially, the concentration of CO_2 starts increasing from point **a** to point **b** as the injection path passes through the V-Aq (orange) region, and no oil is present in the system yet. At point **b**, we notice a shock in the nC_{10} composition as the path enters the V-L (yellow) region for a brief period, then proceeds to the V-L-Aq (green) region at **c**. This behavior can be observed through examining the water composition profiles for both 1-D in **Fig. 10**, where at the injection point **a**, water content is maximum and starts decreasing as the path makes its way out of the V-Aq (orange) region to point **b**. The water composition then starts increasing again in the three-phase region and then stabilizes as it enters the L-Aq (red) region at point **d**.

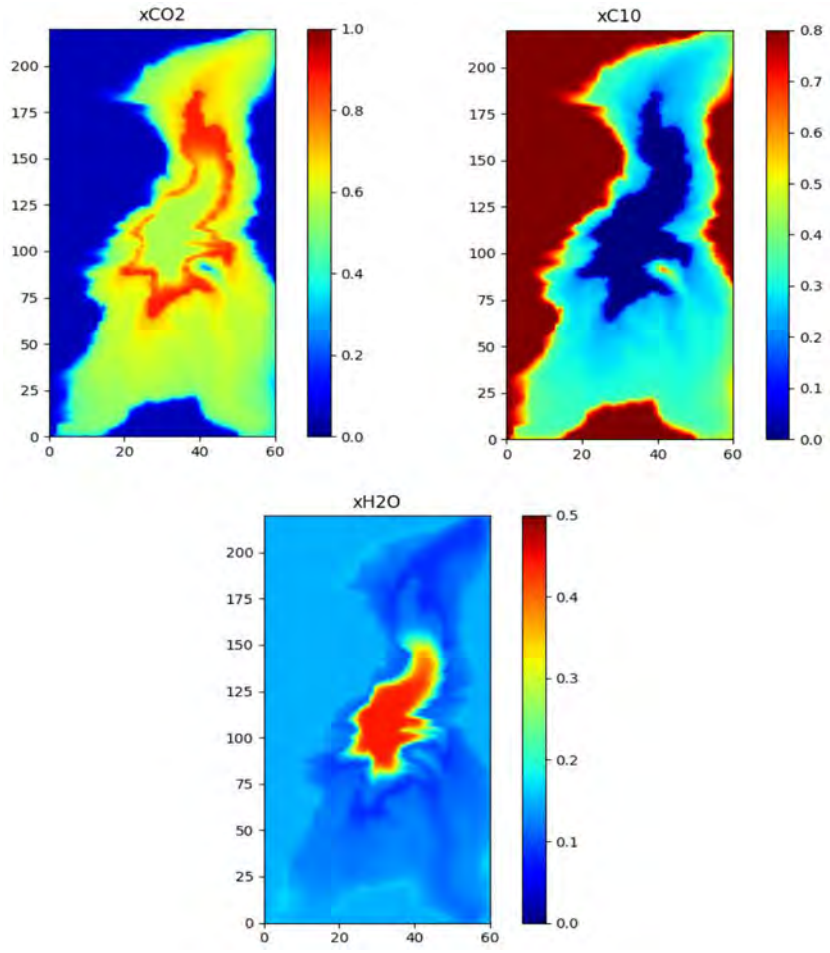

Figure 10—Test II solution profiles of compositions with distance at the end simulation time for 2-D SPE10 model

The traditional approach of modelling three-phase behavior using an equation of state does not accurately represent the partitioning of impurities in the aqueous phase. In general, the presence of impurities decreases CO_2 solubility in brine and affects H_2O contents in non-aqueous phase. In **Fig. 11**, the fraction of dissolved CO_2 in each of the three phases is shown based on the φ-γ approach for the 1-D model. The profile of the dissolved CO_2 in the water phase shows a low solubility of CO_2 with a compositional fraction at around 1.5%, particularly in the V-L-Aq region. A similar trend is noticed in **Fig. 12** where the 2-D maps of the CO_2 solubility is shown. The CO_2 concentration in the vapor phase is highest at the location of the injector well as opposed to the CO_2 of the liquid phase since the area is swept from existing hydrocarbons by the influx of the H_2O - CO_2 mixture. Some pockets are seen in the water phase map indicating a V-L region where water does not exist for CO_2 to dissolve in.

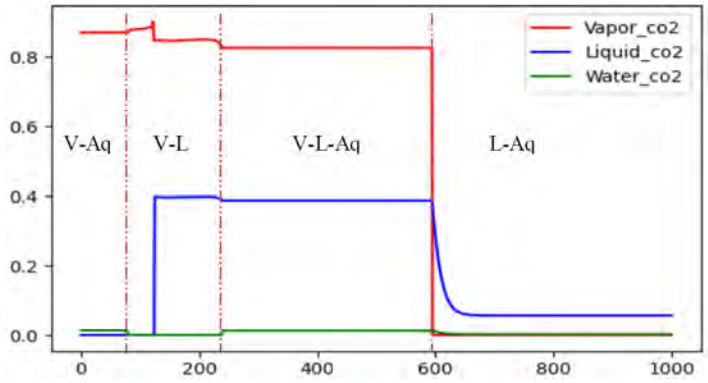

Figure 11—The fraction of dissolved CO2 in each of the Vapor, liquid, and the aqueous phases for the 1-D model

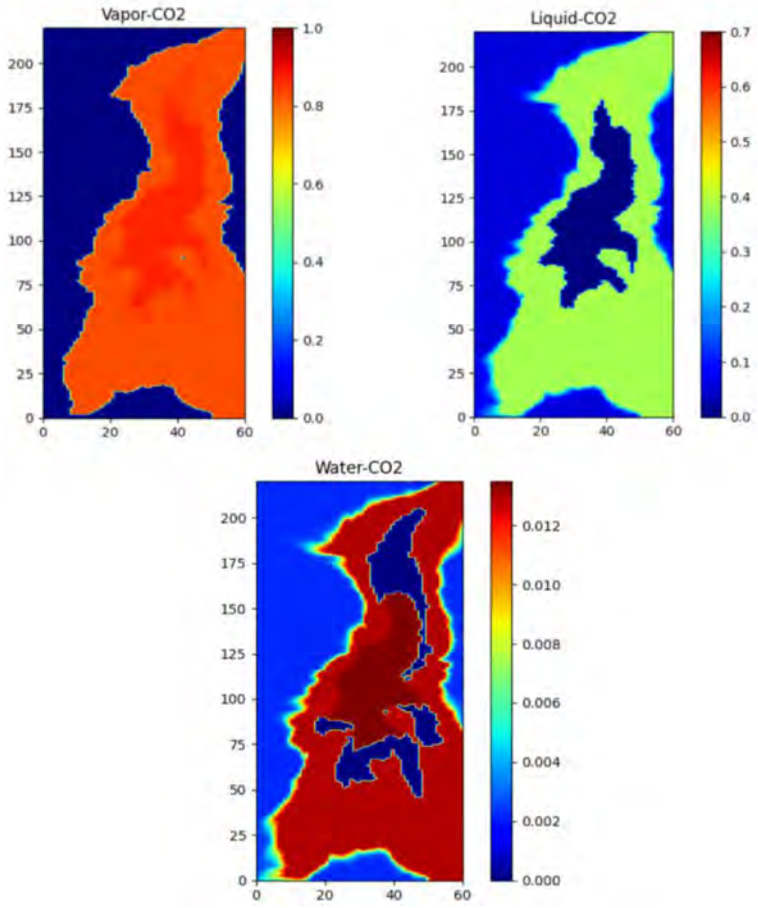

Figure 12—The 2-D maps of the dissolution of CO2 in each flowing phase for the 2D SPE-10 model

Concluding Remarks

An accurate phase behavior prediction in a three-phase (Oil/Gas/Water) system entails solving the system of nonlinear equations in a multistage flash scheme utilizing efficient and robust phase stability testing. The minimization of the TPD function allows determining the number of existing phases in the system. If a phase is missing during a three-phase negative flash, then a two-phase flash is performed to determine the equilibrium phase distribution. The implemented thermodynamic procedure relies on the conventional cubic equation of state (EoS) models to establish an equilibrium relation between the liquid and the gaseous hydrocarbon phases. As for the activity model in the aqueous phase, the liquid phase partitioning is expressed in terms of a proper activity model. Another set of phase partitioning can be hence derived

relating the equilibrium ratios of the gaseous and the aqueous phase. The phase partitioning of the water component is treated separately to account for the effect of dissolved salts and other chemical properties of the brine. Eventually, we end up with sets of algebraic relations for all phases of the system and use a negative flash procedure to solve the partitioning of the liquid, vapor, and aqueous phases.

The three-phase negative flash algorithm is validated against data from the available literature. The variations in the pressure and temperate of a particular mixture cause the appearance and disappearance of phases of which the model captures accurately. The multiphase flash procedure is implemented to generate linearized physical properties by using an Operator Based Linearization (OBL) modelling technique allowing for the combination of multiple complex physics in the nonlinear solution of governing equations. The final package is integrated into a fully implicit reservoir simulator and applied to different scenarios of CO_2 and H_2O injection in 1-D and 2-D models. The concentration profiles of the compositions and their projection on the ternary diagrams were in high agreement, thus proving the ability of the package to simulate full-field cases with real petrophysical properties.

In the next stage, the simulation analysis will be further extended to include mixtures with multiple components for multilayered 3-D field models. Many problems such as the geological storage of CO_2 in depleted hydrocarbon reservoirs and reactive transport analysis through tracking the composition of ions in the brine phase can be investigated upon the multiphase flash package.

Acknowledgments

This publication was supported by the National Priorities Research Program grant NPRP11S-1210-170079 from Qatar National Research Fund.

References

1. Abd, A., & Abushaikha, A. (2021). Reactive transport in porous media: a review of recent mathematical efforts in modeling geochemical reactions in petroleum subsurface reservoirs. *SN Applied Sciences*, **3**(4). doi: 10.1007/s42452-021-04396-9
2. Abd, A., Zhang, N., & Abushaikha, A. (2021). Modeling the effects of capillary pressure with the presence of full tensor permeability and discrete fracture models using the mimetic finite difference method. *Transport In Porous Media*. doi: 10.1007/s11242-021-01585-3
3. Abushaikha, A. S., Voskov, D. V., & Tchelepi, H. A. (2017). Fully Implicit Mixed Hybrid Finite-Element Formulation for General-Purpose Compositional Reservoir Simulation. In SPE Reservoir Simulation Conference. Society of Petroleum Engineers. doi.org/10.2118/182697-MS
4. Abushaikha, A., & Terekhov, K. (2020). "A fully implicit mimetic finite difference scheme for general purpose subsurface reservoir simulation with full tensor permeability." *Journal of Computational Physics*, p. 109194. ISSN: 0021-9991.
5. Akinfiev, N., & Diamond, L. (2003). Thermodynamic description of aqueous nonelectrolytes at infinite dilution over a wide range of state parameters. *Geochimica Et Cosmochimica Acta*, **67**(4), 613–629. doi: 10.1016/s0016-7037(02)01141-9
6. Ammar, M., & Renon, H. (1987). The isothermal flash problem: New methods for phase split calculations. *Aiche Journal*, **33**(6), 926–939. doi: 10.1002/aic.690330606
7. Baker, L., Pierce, A., & Luks, K. (1982). Gibbs Energy Analysis of Phase Equilibria. *Society Of Petroleum Engineers Journal*, **22**(05), 731–742. doi: 10.2118/9806-pa
8. Ballard, A (2002). A non-ideal hydrate solid solution model for a multiphase equilibria program. *Technical report*. Colorado School of Mines.
9. Cañas-Marín, W., Ortiz-Arango, J., Guerrero-Aconcha, U., & Hernandez-Báez, S. (2007). Improved Two-Sided Tangent Plane Initialization and Two-Phase-Split Calculations. *Industrial & Engineering Chemistry Research*, **46**(16), 5429–5436. doi: 10.1021/ie061361b

10. Fine, R., & Millero, F. (1973). Compressibility of water as a function of temperature and pressure. *The Journal Of Chemical Physics*, **59**(10), 5529–5536. doi: 10.1063/1.1679903
11. Frost, A., & Kalkwarf, D. (1953). A Semi-Empirical Equation for the Vapor Pressure of Liquids as a Function of Temperature. *The Journal Of Chemical Physics*, **21**(2), 264–267. doi: 10.1063/1.1698871
12. Gautam, R., & Seider, W. (1979). Computation of phase and chemical equilibrium: Part I. Local and constrained minima in Gibbs free energy. *Aiche Journal*, **25**(6), 991–999. doi: 10.1002/aic.690250610
13. Harvey, A. (1996). Semi-empirical correlation for Henry's constants over large temperature ranges. *Aiche Journal*, **42**(5), 1491–1494. doi: 10.1002/aic.690420531
14. Harvey, A. (1996). Semi-empirical correlation for Henry's constants over large temperature ranges. *Aiche Journal*, **42**(5), 1491–1494. doi: 10.1002/aic.690420531
15. Harvey, A., & Sengers, J. (1990). Correlation of aqueous Henry's constants from 0°c to the critical point. *Aiche Journal*, **36**(4), 539–546. doi: 10.1002/aic.690360405
16. Heidemann, R. (1974). Three-phase equilibria using equations of state. *Aiche Journal*, **20**(5), 847–855. doi: 10.1002/aic.690200504
17. Hjeij, D., & Abushaikha, A. (2019a). Comparing Advanced Discretization Methods for Complex Hydrocarbon Reservoirs. In SPE Reservoir Characterisation and Simulation Conference and Exhibitions. Society of Petroleum Engineers. doi.org/10.2118/196727-MS
18. Hoteit, H., & Firoozabadi, A. (2006). Simple phase stability-testing algorithm in the reduction method. *Aiche Journal*, **52**(8), 2909–2920. doi: 10.1002/aic.10908
19. IEA (2020), *World Energy Outlook 2020*, IEA, Paris https://www.iea.org/reports/world-energy-outlook-2020
20. Iranshahr, A., Voskov, D., & Tchelepi, H. (2010a). Generalized negative-flash method for multiphase multicomponent systems. *Fluid Phase Equilibria*, **299**(2), 272–284. doi: 10.1016/j.fluid.2010.09.022
21. Iranshahr, A., Voskov, D., & Tchelepi, H. (2010b). Tie-Simplex Parameterization for EOS-Based Thermal Compositional Simulation. *SPE Journal*, **15**(02), 545–556. doi: 10.2118/119166-pa
22. Iranshahr, A., Voskov, D., & Tchelepi, H. (2012). Tie-simplex based compositional space parameterization: Continuity and generalization to multiphase systems. *Aiche Journal*, **59**(5), 1684–1701. doi: 10.1002/aic.13919
23. Kala, K., & Voskov, D. (2020). Element balance formulation in reactive compositional flow and transport with parameterization technique. *Computational Geosciences*, **24**(02), 609–624. https://doi.org/10.1007/s10596-019-9828-y
24. Khait, M., & Voskov, D. (2018a). Adaptive Parameterization for Solving of Thermal/Compositional Nonlinear Flow and Transport With Buoyancy. *SPE Journal*, **23**(02), 522–534. doi: 10.2118/182685-pa
25. Khait, M., & Voskov, D. (2018b). Operator-based linearization for efficient modeling of geothermal processes. *Geothermics*, **74**, 7–18. doi: 10.1016/j.geothermics.2018.01.012
26. King, M., Mubarak, A., Kim, J., & Bott, T. (1992). The mutual solubilities of water with supercritical and liquid carbon dioxides. *The Journal Of Supercritical Fluids*, **5**(4), 296–302. doi: 10.1016/0896-8446(92)90021-b
27. Leibovici, C., & Nichita, D. (2008). A new look at multiphase Rachford–Rice equations for negative flashes. *Fluid Phase Equilibria*, **267**(2), 127–132. doi: 10.1016/j.fluid.2008.03.006
28. Li, L., Abushaikha, A. (2020). An Advanced Parallel Framework for Reservoir Simulation with Mimetic Finite Difference Discretization and Operator-based Linearization. In ECMOR XVII-17th European Conference on the Mathematics of Oil Recovery.

29. Li, L., Khait, M., Voskov, D., Abushaikha, A. (2020). Parallel Framework for Complex Reservoir Simulation with Advanced Discretization and Linearization Schemes. *In SPE EAGE EUROPEC. Society of Petroleum Engineers*. https://doi.org/10.2118/200615-MS
30. Li, R., & Li, H. (2019). Improved three-phase equilibrium calculation algorithm for water/hydrocarbon mixtures. *Fuel*, **244**, 517–527. doi: 10.1016/j.fuel.2019.02.026
31. Li, Y., & Nghiem, L. (1982). The Development of a General Phase Envelope Construction Algorithm for Reservoir Fluid Studies. SPE Annual Technical Conference And Exhibition. doi: 10.2118/11198-ms
32. Li, Y., & Nghiem, L. (1986). Phase equilibria of oil, gas and water/brine mixtures from a cubic equation of state and henry's law. *The Canadian Journal Of Chemical Engineering*, **64**(3), 486–496. doi: 10.1002/cjce.5450640319
33. Li, Z., & Firoozabadi, A. (2012). General Strategy for Stability Testing and Phase-Split Calculation in Two and Three Phases. *SPE Journal*, **17**(04), 1096–1107. doi: 10.2118/129844-pa
34. Luks, K., Fitzgibbon, P., & Banchero, J. (1976). Correlation of the Equilibrium Moisture Content of Air and of Mixtures of Oxygen and Nitrogen for Temperatures in the Range of 230 to 600 K at Pressures up to 200 Atm. *Industrial & Engineering Chemistry Process Design And Development*, **15**(2), 326–332. doi: 10.1021/i260058a019
35. Lyu, X., Khait, M., and Voskov, D. (2021). Operator-based linearization approach for modelling of multiphase flow with buoyancy and capillarity. *SPE Journal*.
36. Mehra, R., Heidemann, R., & Aziz, K. (1982). Computation of Multiphase Equilibrium For Compositional Simulation. *Society Of Petroleum Engineers Journal*, **22**(01), 61–68. doi: 10.2118/9232-pa
37. Mehra, R., Heidemann, R., & Aziz, K. (1982). Computation of Multiphase Equilibrium For Compositional Simulation. *Society Of Petroleum Engineers Journal*, **22**(01), 61–68. doi: 10.2118/9232-pa
38. Michelsen, M. (1982). The isothermal flash problem. Part I. Stability. *Fluid Phase Equilibria*, **9**(1), 1–19. doi: 10.1016/0378-3812(82)85001-2
39. Michelsen, M. (1982). The isothermal flash problem. Part II. Phase-split calculation. *Fluid Phase Equilibria*, **9**(1), 21–40. doi: 10.1016/0378-3812(82)85002-4
40. Michelsen, M. (1994). A simple method for calculation of approximate phase boundaries. *Fluid Phase Equilibria*, **98**, 1–11. doi: 10.1016/0378-3812(94)80104-5
41. Michelsen, M., Mollerup, J., & Breil, M. (2008). Thermodynamic Models: Fundamental and Computational Aspects. *Fluid Phase Equilibria*, **240**(2), 227–228. doi: 10.1016/j.fluid.2005.11.032
42. Mokhatab, S. (2003). Three-Phase Flash Calculation for Hydrocarbon Systems Containing Water. *Theoretical Foundations Of Chemical Engineering*, **37**(3), 291–294. doi: 10.1023/a:1024043924225
43. Nardean, S, Ferronato, M., Abushaikha, A. (2020). A novel and an efficient preconditioner for solving Lagrange multipliers-based discretization schemes for reservoir simulation. In ECMOR XVII-17th European Conference on the Mathematics of Oil Recovery.
44. Nasrifar, K., & Moshfeghian, M. (2002). Liquid–liquid equilibria of water–hydrocarbon systems from cubic equations of state. *Fluid Phase Equilibria*, **193**(1-2), 261–275. doi: 10.1016/s0378-3812(01)00743-9
45. Neoschil, J., & Chambrette, P. (1978, January 1). *Converge Pressure Concept A Key For High Pressure Equilibria*. Society of Petroleum Engineers.

46. Nghiem, L. X., Heidemann, R. A., & Computer Modelling Group. (1982). *General acceleration procedure for multiphase flash calculation with application to oil-gas-water systems*. Calgary: Computer Modelling Group.
47. Nghiem, L., Aziz, K., & Li, Y. (1983). A Robust Iterative Method for Flash Calculations Using the Soave-Redlich-Kwong or the Peng-Robinson Equation of State. *Society Of Petroleum Engineers Journal*, **23**(03), 521–530. doi: 10.2118/8285-pa
48. Peng, D., & Robinson, D. (1976). A New Two-Constant Equation of State. *Industrial & Engineering Chemistry Fundamentals*, **15**(1), 59–64. doi: 10.1021/i160057a011
49. Peng, D., & Robinson, D. (1980). Two- and Three-Phase Equilibrium Calculations for Coal Gasification and Related Processes. *Thermodynamics Of Aqueous Systems With Industrial Applications*, 393–414. doi: 10.1021/bk-1980-0133.ch020
50. Perez, R., & Heidemann, R. (2006). Coupling an equation of state and Henry's Law to model the phase equilibria of gases and brines. *Journal Of Geochemical Exploration*, **89**(1-3), 331–334. doi: 10.1016/j.gexplo.2005.11.083
51. Poling, B., Prausnitz, J., & O'Connell, J. (2007). *The properties of gases and liquids*. Boston: McGraw-Hill.
52. Rachford, H., & Rice, J. (1952). Procedure for Use of Electronic Digital Computers in Calculating Flash Vaporization Hydrocarbon Equilibrium. *Journal Of Petroleum Technology*, **4**(10), 19–3. doi: 10.2118/952327-g
53. Rachford, H., & Rice, J. (1952). Procedure for Use of Electronic Digital Computers in Calculating Flash Vaporization Hydrocarbon Equilibrium. *Journal Of Petroleum Technology*, **4**(10), 19–3. doi: 10.2118/952327-g
54. Redlich, O., & Kwong, J. (1949). On the Thermodynamics of Solutions. V. An Equation of State. Fugacities of Gaseous Solutions. *Chemical Reviews*, **44**(1), 233–244. doi: 10.1021/cr60137a013
55. Reshadi, P., Nasrifar, K., & Moshfeghian, M. (2011). Evaluating the phase equilibria of liquid water+natural gas mixtures using cubic equations of state with asymmetric mixing rules. *Fluid Phase Equilibria*, **302**(1-2), 179–189. doi: 10.1016/j.fluid.2010.08.007
56. Rogers, P., & Pitzer, K. (1982). Volumetric Properties of Aqueous Sodium Chloride Solutions. *Journal Of Physical And Chemical Reference Data*, **11**(1), 15–81. doi: 10.1063/1.555660
57. Saul, A., & Wagner, W. (1987). International Equations for the Saturation Properties of Ordinary Water Substance. *Journal Of Physical And Chemical Reference Data*, **16**(4), 893–901. doi: 10.1063/1.555787
58. Saul, A., & Wagner, W. (1987). International Equations for the Saturation Properties of Ordinary Water Substance. *Journal Of Physical And Chemical Reference Data*, **16**(4), 893–901. doi: 10.1063/1.555787
59. Shibue, Y. (2003). Vapor pressures of aqueous NaCl and CaCl2 solutions at elevated temperatures. *Fluid Phase Equilibria*, **213**(1-2), 39–51. doi: 10.1016/s0378-3812(03)00284-x
60. Soave, G. (1972). Equilibrium constants from a modified Redlich-Kwong equation of state. *Chemical Engineering Science*, **27**(6), 1197–1203. doi: 10.1016/0009-2509(72)80096-4
61. Spycher, N., & Pruess, K. (2005). CO2-H2O mixtures in the geological sequestration of CO2. II. Partitioning in chloride brines at 12–100°C and up to 600 bar. *Geochimica Et Cosmochimica Acta*, **69**(13), 3309–3320. doi: 10.1016/j.gca.2005.01.015
62. Voskov, D. (2017). Operator-based linearization approach for modeling of multiphase multi-component flow in porous media. *Journal of Computational Physics*, **337**, 275–288. doi: 10.1016/j.jcp.2017.02.041

63. Voskov, D., & Tchelepi, H. (2009). Tie-simplex based mathematical framework for thermodynamical equilibrium computation of mixtures with an arbitrary number of phases. *Fluid Phase Equilibria*, **283**(1-2), 1–11. doi: 10.1016/j.fluid.2009.04.018
64. Wapperom, M. (2019). Predictive Modelling of Hydrate Formation and Dissociation. Masters Thesis., Delft University Of Technology.
65. Whitson, C., & Michelsen, M. (1989). The negative flash. *Fluid Phase Equilibria*, **53**, 51–71. doi: 10.1016/0378-3812(89)80072-x
66. Whitson, C., & Michelsen, M. (1989). The negative flash. *Fluid Phase Equilibria*, **53**, 51–71. doi: 10.1016/0378-3812(89)80072-x
67. Wilson, G. (1968). A Modified Redlich-Kwong EOS, Application to General Physical Data Calculations. *American Institute of Chemical Engineers* 65th National Meeting, Paper No. 15C.
68. Zaydullin, R., Voskov, D., & Tchelepi, H. (2012). Nonlinear Formulation Based on an Equation-of-State Free Method for Compositional Flow Simulation. *SPE Journal*, **18**(02), 264–273. doi: 10.2118/146989-pa
69. Zaydullin, R., Voskov, D.V., Tchelepi, H.A. (2016) Phase-state identification bypass method for three-phase thermal compositional simulation, *Computational Geosciences*, **20** (3), pp. 461–474. doi: 10.1007/s10596-015-9510-y
70. Zhang, N., Abushaikha, A. (2019a). Mimetic finite difference simulation of multiphase flow in carbonate fractured media in presence of capillary pressure. The Third EAGE Workshop on Well Injectivity & Productivity in Carbonates, Doha, Qatar.
71. Hjeij, D., & Abushaikha, A. (2019b). An Investigation of the Performance of the Mimetic Finite Difference Scheme for Modelling Fluid Flow in Anisotropic Hydrocarbon Reservoirs. SPE Europec featured at 81st EAGE Conference and Exhibition, London, England, UK, June 2019. doi: 10.2118/195496-ms
72. Zhang, N., & Abushaikha, A. (2019b). Fully Implicit Reservoir Simulation Using Mimetic Finite Difference Method in Fractured Carbonate Reservoirs. SPE Reservoir Characterisation and Simulation Conference and Exhibition, Abu Dhabi, UAE, September 2019. doi: 10.2118/196711-ms

Appendix A
Pitzer Parameters

Table A-1—Pitzer parameters for the second-order parameter $\lambda_{i\text{-}Na}$ of the activity coefficients

Cont.	CO2	H2S	N2	C1	C2	C3	C4
c_1	−0.0652869	1.03658689	−2.0939363	−5.4066455E-1	−2.143686	0.513068	0.52862384
c_2	1.6790636E-4	−1.1784797E-3	3.1445269E-3	7.2997588E-4	2.598765E-3	−0.000958	−1.0298104E-3
c_3	40.838951	−1.7754826E+2	3.9139160E2	1.5176903E2	4.6942351E+2	0	0
c_4	0	−4.5313285E-4	0	3.1927112E-5	−4.6849541E-5	0	0
c_5	0	0	−1.5918098E-5	0	0	0	0
c_6	−3.9266518E-2	0	0	−1.642651E-5	0	0	0
c_7	0	0	0	0	0	0	0
c_8	2.1157167E-2	0	0	0	0	0	0
c_9	6.5486487E-6	0	0	0	0	0	0
c_{10}	0	0.4775165E+2	0	0	0	0	0
c_{11}	0	0	0	0	−8.4616602E-10	0	0
c_{12}	0	0	0	0	1.095219E-6	0	0

Table A-2—Pitzer parameters for the third-order parameter $\xi_{i\text{ - }Na\text{ - }Cl}$ of the activity coefficients

Cont.	CO2	H2S	N2	C1	C2	C3	C4
c_1	−1.144624E-2	0.010274152	−6.3981858E-3	−2.9990084E-3	−1.0165947E-2	−0.007485	0.0206946
c_2	2.8274958E-5	0	0	0	0	0	0
c_3	0	0	0	0	0	0	0
c_4	0	0	0	0	0	0	0
c_5	0	0	0	0	0	0	0
c_6	1.3980876E-2	0	0	0	0	0	0
c_7	0	0	0	0	0	0	0
c_8	−1.4349005E-2	0	0	0	0	0	0
c_9	0	0	0	0	0	0	0
c_{10}	0	0	0	0	0	0	0
c_{11}	0	0	0	0	0	0	0
c_{12}	0	0	0	0	0	0	0